Available online at www.sciencedirect.com
ScienceDirect
International Journal of Machine Tools & Manufacture 47 (2007) 658–665
INTERNATIONAL JOURNAL OF MACHINE TOOLS & MANUFACTURE DESIGN, RESEARCH AND APPLICATION
www.elsevier.com/locate/ijmactool

Coordinate metrology uncertainty using parallel kinematic techniques

J. Suzanne Canning, John C. Ziegert*, Tony L. Schmitz

Department of Mechanical and Aerospace Engineering, University of Florida, POB 116300, Gainesville, FL 32611, USA

Received 25 May 2005; received in revised form 20 March 2006; accepted 26 April 2006
Available online 16 June 2006

Abstract

Dimensional metrology of manufactured objects is increasingly performed with coordinate measuring machines, where coordinates of surface points are recorded and fit to a model of the ideal surface. While coordinate metrology is often performed using machines with a serial Cartesian kinematic structure, the use of parallel kinematic machines has also been investigated. In this paper, we evaluate the uncertainty of trilateration measurements, which is the simplest form of parallel kinematic metrology for spatial coordinates. The instrument studied here is the laser ball bar, specifically designed for trilateration measurements. We use homogeneous transformation matrices to determine its length uncertainty. Monte Carlo simulation is then applied to model the coordinate uncertainty arising from propagation of the length uncertainty through the trilateration calculations. Simulation is compared to experimental results.

Keywords: Laser ball bar; Uncertainty; Coordinate metrology; Parallel kinematics

1. Introduction

Definition of the measurand is the first step in performing a measurement uncertainty analysis. In many cases, the measurand, or quantity being measured, is not observed directly, but is a mathematical function of multiple input quantities. The computation of measurement uncertainty from the uncertainties of the input quantities is then a relatively straightforward procedure as outlined in Ref. [1].

It is well known that incomplete definition of the measurand can result in significant measurement error and uncertainty, see Ref. [9]. In general, as the measurement instrument or system becomes more complex, the number of input quantities increases and correct definition of the measurand becomes more problematic. For spatial coordinate measurements performed using trilateration, there exists a hierarchy of inputs, each of which has its own uncertainty and contributes to the overall uncertainty of the measured coordinates.

This paper describes a method for developing uncertainty analyses for parallel kinematic metrology systems which use trilateration to measure spatial coordinates. Previous work in this area has been performed by Sandwith and Predmore [2], Navidi et al. [3], and Lee and Ferreira [4]. We analyze the laser ball bar (LBB) introduced by Ziegert and Mize [5], and Schmitz and Ziegert [6], an instrument developed specifically for spatial metrology using trilateration, and demonstrate the use of homogenous transformation matrices (HTMs) as a tool to aid in performing the uncertainty analysis in a manner similar to that shown by Davies and Schmitz [7]. Monte Carlo simulations are performed to examine propagation of the length uncertainty into uncertainty of the measured coordinates. Simulation results are compared to LBB accuracy tests performed on the Moore M-60 coordinate measuring machine (CMM) at BWXT Y-12, Oak Ridge, TN.

2. Trilateration with the LBB

The LBB is an instrument designed to evaluate the positioning accuracy of machining centers by direct measurement of tool point coordinates relative to the work surface over the machine's working volume. The LBB is a multi-stage telescoping tube assembly with precision tooling balls located at each end (Fig. 1). A fiber optic-fed displacement measuring laser interferometer (DMI) is aligned with the LBB motion axis and records changes in

*Corresponding author. Tel.: +1 352 392 9930; fax: +1 352 392 1071.
E-mail address: johnz@ufl.edu (J.C. Ziegert).

0890-6955/$ - see front matter © 2006 Elsevier Ltd. All rights reserved.
doi:10.1016/j.ijmachtools.2006.04.010

its length (the DMI 'moving' retroreflector is located at the end of the inner tube near the right ball, while the 'fixed' retroreflector is carried in the optics package at the left end of the LBB). However, in order to measure distances between the ball centers, the LBB must be initialized to a known length. This is accomplished using the three-step initialization process depicted in Fig. 2.

As shown in Fig. 3, the LBB measures spatial coordinates using trilateration. Three magnetic sockets, designed to mate with the tooling balls on the LBB ends, are attached to the machine worktable and a fourth is fixed at the tool point. These four sockets form the vertices of a tetrahedron. If the lengths of the six sides of the tetrahedron are measured, the $\{x,y,z\}$ coordinates of the 'tool' socket relative to a coordinate system defined by the three 'base' sockets can be computed.

$$x = \frac{L_1^2 - L_2^2 + L_{B1}^2}{2L_{B1}} \qquad c_b = \sqrt{L_{B3}^2 - x_b^2}$$
$$y = \frac{d_1^2 - L_3^2 + c_b^2}{2c_b}, \quad \text{where} \quad x_b = \frac{L_{B3}^2 - L_{B2}^2 + L_{B1}^2}{2L_{B1}} \qquad (1)$$
$$z = \sqrt{c_1^2 - y^2} \qquad d_1 = \sqrt{c_1^2 + (x_b - x)^2}$$
$$c_1 = \sqrt{L_1^2 - x^2}$$

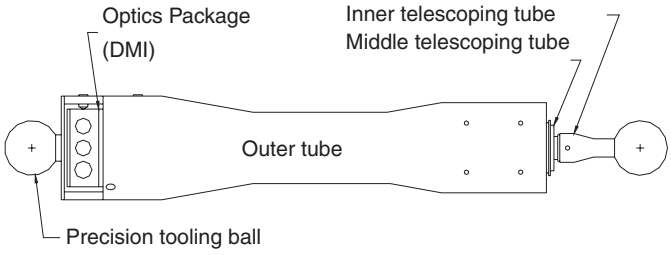

Fig. 1. Laser ball bar schematic.

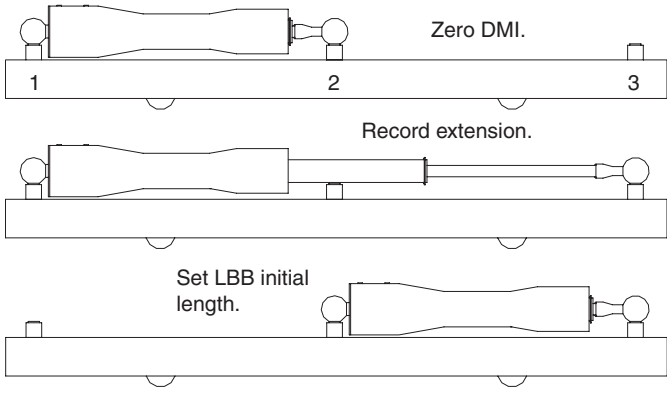

Fig. 2. LBB initialization procedure.

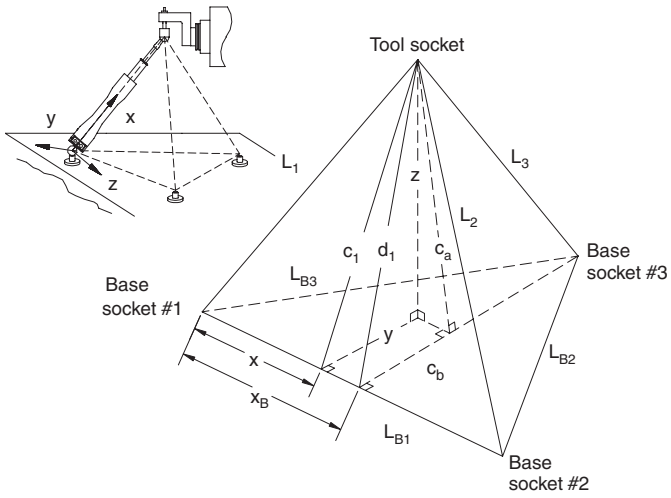

Fig. 3. Trilateration diagram for Eq. (1).

2.1. Measurand definition

As noted, the spatial coordinates of the tool socket center are determined via trilateration using six LBB length measurements (i.e., the six tetrahedron sides). The relevant trilateration equations are provided in Eq. (1). However, because the LBB DMI can only record length changes, the tetrahedron sides are obtained by adding the initialization length (obtained in the final step of Fig. 2), L_0, to the length change, ΔL, measured by the DMI when the LBB is removed from the initialization fixture and placed between a pair of sockets. Therefore, we must define four individual terms in order to obtain the coordinates of the tool socket center:

1. ΔL: the true length change of the LBB from some initial configuration to a final configuration (function of the DMI reading);
2. L_0: the initialization length for a given initialization fixture design (function of ΔL recorded during step 2 of the initialization sequence shown in Fig. 2);
3. L_i: the lengths of the six sides of the tetrahedron (functions of L_0 and ΔL); and
4. $\{x_i, y_i, z_i\}$: the target point coordinates (functions of L_i, $i = 1-6$).

Due to the 'layered' nature of the LBB trilateration process, each coordinate measurement is affected by uncertainties in: (1) the displacement recorded by the LBB DMI; (2) the initialization procedure; and (3) LBB length changes during measurement of the tetrahedron edges (due to the LBB mechanics). These uncertainties then propagate through Eq. (1) to create corresponding uncertainties in the spatial coordinates of the target point.

The uncertainty contributors are broadly categorized and modeled in the following paragraphs. For each uncertainty source identified, we choose an appropriate statistical distribution based on the physical characteristics of the system, manufacturing tolerances, and engineering judgment. We then determine the uncertainty of LBB coordinate measurements using Monte Carlo simulation.

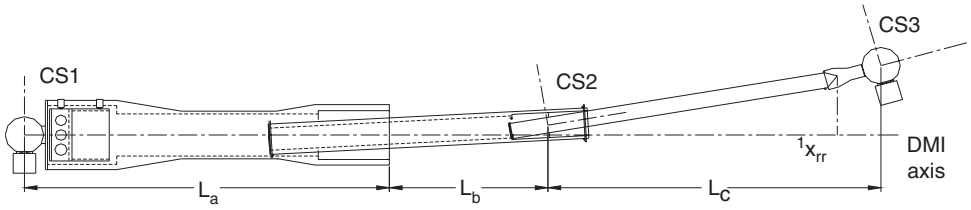

Fig. 4. Coordinate system definitions for two-axis HTM model of LBB (misalignments are exaggerated).

3. Error modeling

3.1. Mechanical errors

The LBB is composed of three ideally rigid bodies which move relative to each other: (1) the outer tube which holds the left ball and the DMI; (2) the middle tube which carries the inner tube; and (3) the inner tube which holds the moving retroreflector for the DMI and the right ball (see Fig. 1). Nominally, the two prismatic joints provide error-free, coaxial, straight-line motion; the interferometer axis is perfectly aligned with this motion; and there are no gravitational or thermal deformations of the bodies. In the real system, however, the joints are misaligned; they do not provide perfect motion; and the individual bodies are subject to deformations.

The mechanical errors of the LBB are modeled using HTMs, treating the LBB as a two-axis mechanical system. Fig. 4 shows a schematic of the LBB with coordinate systems assigned (misalignments between components are greatly exaggerated). Coordinate system 1 (CS1) is chosen to have its origin coincident with the left ball center and its x-axis parallel to the measurement axis of the DMI. Coordinate system 2 (CS2) is attached to the middle tube with its origin at the center of the linear bearing which supports the inner tube and its x-axis parallel to the bearing axis. The origin of the third coordinate system (CS3) is at the right ball center with the x-axis passing through the apex of the moving retroreflector. In all cases, the z-axis is taken to be perpendicular to the DMI axis and lies in the horizontal plane (Fig. 1).

The goal of the HTM model is to determine the actual coordinates of the retroreflector apex and the right ball center relative to CS1 for any configuration of the LBB. The x-coordinate of the retroreflector apex is the effective measurement point of the DMI, while the coordinates of the right ball center are used to compute the actual LBB length. The nominal model, provided in Eq. (2), is a function of the three section lengths, L_a, L_b, and L_c, measured along the DMI axis as shown in Fig. 4. The mechanical and alignment errors are modeled using HTMs to give the actual relationship between CS3 and CS1 as shown in Eq. (3).

$$
{}^1T_{3,\mathrm{nom}} = {}^1T_{2,\mathrm{nom}}{}^2T_{3,\mathrm{nom}} = \begin{bmatrix} 1 & 0 & 0 & L_a+L_b \\ 0 & 1 & 0 & 0 \\ 0 & 0 & 1 & 0 \\ 0 & 0 & 0 & 1 \end{bmatrix} \begin{bmatrix} 1 & 0 & 0 & L_c \\ 0 & 1 & 0 & 0 \\ 0 & 0 & 1 & 0 \\ 0 & 0 & 0 & 1 \end{bmatrix}. \tag{2}
$$

3.1.1. Gravitational deflections

For any nominal pose of the LBB, the gravitational deflections are obtained by modeling it as a simply supported, stepped cross-section beam. Castigliano's method is used to predict the displacement, δ_y, and z-axis rotation, ε_z, of CS2 relative to CS1 and CS3 relative to CS2. The nominal dimensions and material properties of the LBB are used in the deflection calculations in combination with the nominal overall length and angle relative to gravity. In practice, the middle tube of the LBB is not fully constrained and may take a range of positions whenever the total LBB length is between its minimum and maximum lengths. To account for this, the position of the middle tube is treated as an additional random input with a uniform distribution bounded by the limiting positions.

$$
{}^1T_3 = {}^1T_{2,\mathrm{nom}}E_2{}^2T_{3,\mathrm{nom}}E_3 = \begin{bmatrix} 1 & 0 & 0 & L_a+L_b \\ 0 & 1 & 0 & 0 \\ 0 & 0 & 1 & 0 \\ 0 & 0 & 0 & 1 \end{bmatrix} \begin{bmatrix} 1 & -\varepsilon_{z,2} & \varepsilon_{y,2} & \delta_{x,2} \\ \varepsilon_{z,2} & 1 & -\varepsilon_{x,2} & \delta_{y,2} \\ -\varepsilon_{y,2} & \varepsilon_{x,2} & 1 & \delta_{z,2} \\ 0 & 0 & 0 & 1 \end{bmatrix} \times \begin{bmatrix} 1 & 0 & 0 & L_c \\ 0 & 1 & 0 & 0 \\ 0 & 0 & 1 & 0 \\ 0 & 0 & 0 & 1 \end{bmatrix} \begin{bmatrix} 1 & -\varepsilon_{z,3} & \varepsilon_{y,3} & \delta_{x,3} \\ \varepsilon_{z,3} & 1 & -\varepsilon_{x,3} & \delta_{y,3} \\ -\varepsilon_{y,3} & \varepsilon_{x,3} & 1 & \delta_{z,3} \\ 0 & 0 & 0 & 1 \end{bmatrix}. \tag{3}
$$

3.1.2. Axis motion errors, straightness, and rotation

The middle and inner tubes slide in linear ball bearings which are intended to produce pure rectilinear motion. However, manufacturing tolerances on the shafts cause deviations from this motion and result in translational errors in the y- and z-directions, δ_y and δ_z, and rotational errors about the y- and z-axes, ε_y and ε_z. The straightness errors (lateral error motions of the origins of CS2 and CS3 as the tubes extend) are estimated from the straightness tolerance for the middle and inner tubes prescribed in the design drawings, plus the lateral motion of the CS2 and CS3 origins due to the rotational errors in the bearing (normal distribution assumed). The values are perturbed within the ranges provided in Table 1.

Table 1
LBB axis motion error ranges for Monte Carlo simulation

Middle tube	Inner tube
$\varepsilon_y = \pm 123$ (μrad)	$\varepsilon_y = \pm 57$ (μrad)
$\varepsilon_z = \pm 123$ (μrad)	$\varepsilon_z = \pm 57$ (μrad)
$\delta_y = \pm 5 + \varepsilon_z L_b$ (μm)	$\delta_y = \pm 2.5 + \varepsilon_z L_c$ (μm)
$\delta_z = \pm 5 + \varepsilon_y L_b$ (μm)	$\delta_z = \pm 2.5 + \varepsilon_y L_c$ (μm)

3.1.3. Bearing compliance

After construction, a slight misfit between the shaft and linear bearing permits up to 0.35 mrad of rotation about the z-axis as measured for the assembly used in this study. The direction of this rotation is assumed to be governed by the gravity forces acting on the LBB. When the ball bar is vertical, this angular error is assumed to be zero. The angular motion is added to the z-rotation errors in the HTMs and the motion of the coordinate frame origin produced by this rotation is added to the y-direction displacement error.

3.1.4. Cosine misalignment

Initial misalignment between the DMI and actual motion axis causes a cosine error which is incorporated as straightness error in the y- and z-directions. The error is proportional to the nominal displacement of the LBB and is assumed to be normally distributed with zero mean and standard deviation of 262 μrad (value based on best practice alignment). The direction of misalignment relative to CS1 is treated as a uniformly distributed angle about the DMI axis with zero mean and range of $\pm\pi$ rad.

3.1.5. Retroreflector coordinates in CS1

The coordinates of the retroreflector apex relative to CS1 can be found using the HTM model provided in Eq. (4), where the transformation between coordinate systems 3 and 1, ${}^1T_3$, is given by Eq. (3). The x-coordinate of this vector is the projection of the retroreflector (rr) apex onto the DMI axis (see Fig. 4). Changes in this value are the displacements recorded by the interferometer, i.e., ${}^1x_{rr} - {}^1x_{rr,0}$, where ${}^1x_{rr,0}$ is the projected value at initialization. For a given DMI reading, we seek the true change in distance between ball centers, ΔL_{act}.

$$ {}^1\{P_{rr}\} = {}^1T_3\,{}^3\{P_{rr}\}, \tag{4} $$

$$ \Delta L_{act} = \sqrt{({}^1x_3)^2 + ({}^1y_3)^2 + ({}^1z_3)^2} - \sqrt{({}^1x_{3,0})^2 + ({}^1y_{3,0})^2 + ({}^1z_{3,0})^2}, \tag{5} $$

where $$ {}^1\begin{Bmatrix} x_3 \\ y_3 \\ z_3 \end{Bmatrix} = {}^1\begin{Bmatrix} {}^1T_3(1,4) \\ {}^1T_3(2,4) \\ {}^1T_3(3,4) \end{Bmatrix} $$

and

$$ {}^1\begin{Bmatrix} x_{3,0} \\ y_{3,0} \\ z_{3,0} \end{Bmatrix} = {}^1\begin{Bmatrix} {}^1T_{3,0}(1,4) \\ {}^1T_{3,0}(2,4) \\ {}^1T_{3,0}(3,4) \end{Bmatrix}. $$

are the coordinates of the origin of CS3 as seen in CS1 during a measurement and at initialization, respectively.

3.1.6. Thermal deformations

The unsensed length between the left ball and the DMI beam splitter center, as well as the length between the moving retroreflector apex and the right ball center, is 19.6 mm. The coefficient of thermal expansion (CTE) for the stainless steel components making up these lengths was assumed to be 15 μm/m °C. Because the LBB is handled extensively during use, the temperature of this portion of the LBB is assumed to vary uniformly by up to ±1 °C from the temperature at initialization. If the balls are assumed to be in sockets a fixed distance apart, thermal errors in the unsensed lengths will cause the DMI reading to change (e.g., an increase in temperature will increase the unsensed length and cause a decrease in the DMI reading). In simulation, this error source is treated by perturbing the nominal coordinates of the retroreflector in CS3 by a normally distributed equivalent thermal error with zero mean and standard deviation of 0.147 μm.

3.1.7. Interferometer errors

The interferometer system is subject to a number of well-known error sources including: changes in the air refractive index due to temperature, pressure, humidity, and composition fluctuations; imperfect optical elements; beam shear; and polarization mixing. These errors are, in general, a function of the nominal optical path length and are added to the mechanical and thermal displacement errors already described. Space limitations preclude detailed treatment of these errors here. The interested reader is referred to, for example, Ref. [8]. The DMI errors are assumed to be normally distributed with zero mean and standard deviation of 0.125 μm.

4. Uncertainty computation

4.1. LBB displacement measurement, ΔL

When the LBB is displaced from some initial configuration to another, the DMI reports a value for the length change, ΔL. We estimate the true value of ΔL in the following manner.

1. The initial distance between ball centers is assumed to be known and the coordinates of the moving retroreflector apex in CS1 are calculated using the

HTM model, while accounting for all mechanical error sources.
2. When the LBB is moved to a new configuration, the nominal reported DMI value is corrected to account for the thermal and DMI errors.
3. The corrected DMI value is used in conjunction with the HTM model of mechanical errors to obtain the new coordinates of the right ball center in CS1 which would give this DMI reading (i.e., the right ball position which would cause the moving retroreflector apex to be in the position corresponding to this DMI value).
4. The right ball center coordinates are used to compute the new actual length of the LBB.

The initial length of the LBB is subtracted from the actual length to give the true value of ΔL.

4.2. Initialization errors

As noted, the first step in using the LBB is initialization. When the DMI system is turned on, it has no information about the distance from the beam splitter to the moving retroreflector or the distance between the ball centers. The initialization procedure provides an absolute distance between ball centers, to which subsequent displacements measured by the DMI are added. During initialization, the LBB itself is used to measure the distance between a pair of sockets on the initialization fixture. The LBB is then placed in these sockets and its length is set to this value.

There are two major sources of error in initialization. The LBB measurement of the socket-to-socket distance in the initialization fixture may be in error due to the errors described previously. Also, the three sockets on the fixture may not be collinear (Fig. 5). We assumed a generic misalignment, dy, of up to 0.25 mm (normally distributed with zero mean and standard deviation of 0.125 mm) as dictated by conservative limits of manufacturing capability. For a given nominal distance between sockets 1 and 2, L_{12}, and the corresponding nominal DMI reading, the true distance between sockets 2 and 3, L_{23}, can be estimated as

$$L_{23} = \left[\left(\sqrt{(L_{12} + \Delta L)^2 - \mathrm{d}y^2} - L_{12} \right)^2 + \mathrm{d}y^2 \right]^{1/2}. \quad (6)$$

4.3. Tetrahedron side measurement errors

Following initialization, the LBB is placed between pairs of sockets which form the vertices of the measurement tetrahedron to measure the six inter-socket distances (i.e., the tetrahedron edge lengths), L_i. See Eq. (7). Errors in these distances are combinations of the initialization and displacement measuring errors described previously. Because the lengths between the three base sockets are typically measured once and then assumed to remain constant during subsequent measurements, these lengths are prescribed an additional thermal deformation during the measurement cycle. The thermal deformation is computed based on steel with a CTE of 12 μm/m °C and a uniformly distributed ±1 °C temperature variation.

$$L_i = L_0 + \Delta L_i, \quad i = 1\text{–}6. \quad (7)$$

4.4. Trilateration errors

To determine the mean and standard deviation of the target point spatial coordinates the mean and statistical distribution of the tetrahedron side length measurements (obtained from Monte Carlo simulation) are used as inputs to Eq. (1). Propagation of the side length uncertainties through the trilateration equations are taken to provide the best estimate of the spatial coordinates' uncertainties.

5. Simulation of uncertainty

The Monte Carlo simulation proceeds according to the following steps.

1. A nominal distance between initialization sockets 1 and 2 is assumed and the HTM model is used to compute the coordinates of the retroreflector apex in CS1.
2. A nominal DMI reading corresponding to the distance between sockets 2 and 3 is used to compute the coordinates of socket 3 in CS1 which would give this DMI reading.
3. Eq. (6) is used to determine the true distance between sockets 2 and 3, which is the true value of L_0.
4. Steps 1–3 are repeated 2000 times and the mean and standard deviation of L_0 are computed.
5. A set of nominal base socket locations is chosen along with the nominal coordinates of the target point to be measured. The nominal DMI readings corresponding to

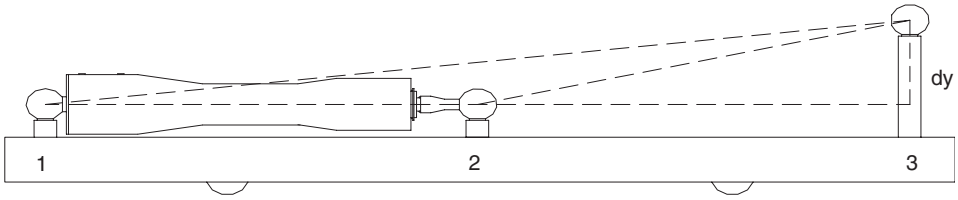

Fig. 5. Initialization socket offset (offset is exaggerated).

the six side measurements are computed and used in the ΔL model to obtain the true LBB length change for each side. Each ΔL is added to a value of L_0 selected from the distribution obtained in step 4.

6. Step 5 is repeated 100 times and the mean and standard deviations of the six side lengths are computed.
7. The coordinates of the target point are computed from a set of side lengths chosen from the distributions obtained in step 6. This is repeated 100 times to obtain a point cloud of possible true values for the measurement point coordinates around the nominal point.
8. A new nominal target point is selected and steps 5–7 are repeated.

Finally, after all of the data has been generated, it is analyzed to compute the variance in the measured coordinates at each point and over the entire workspace.

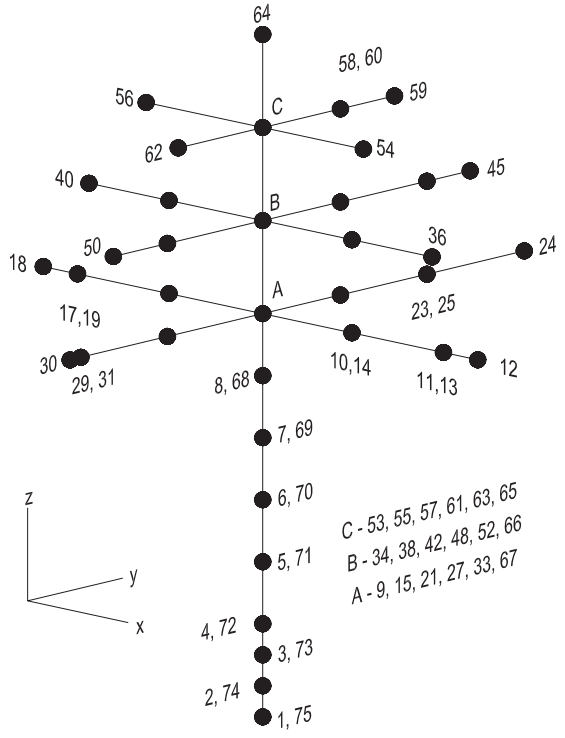

Fig. 6. Measurement points for LBB-CMM comparison.

Table 2
coordinates for selected LBB-CMM measurement points

Point	$\{x, y, z\}$ (mm)
1, 75	281.9, 162.8, 0
12	520.7, 162.8, 330.2
24	281.9, 469.9, 330.2
36	469.9, 162.8, 406.4
45	281.9, 406.4, 406.4
54	393.7, 162.8, 482.6
59	281.9, 317.5, 482.6
64	281.9, 162.8, 558.8

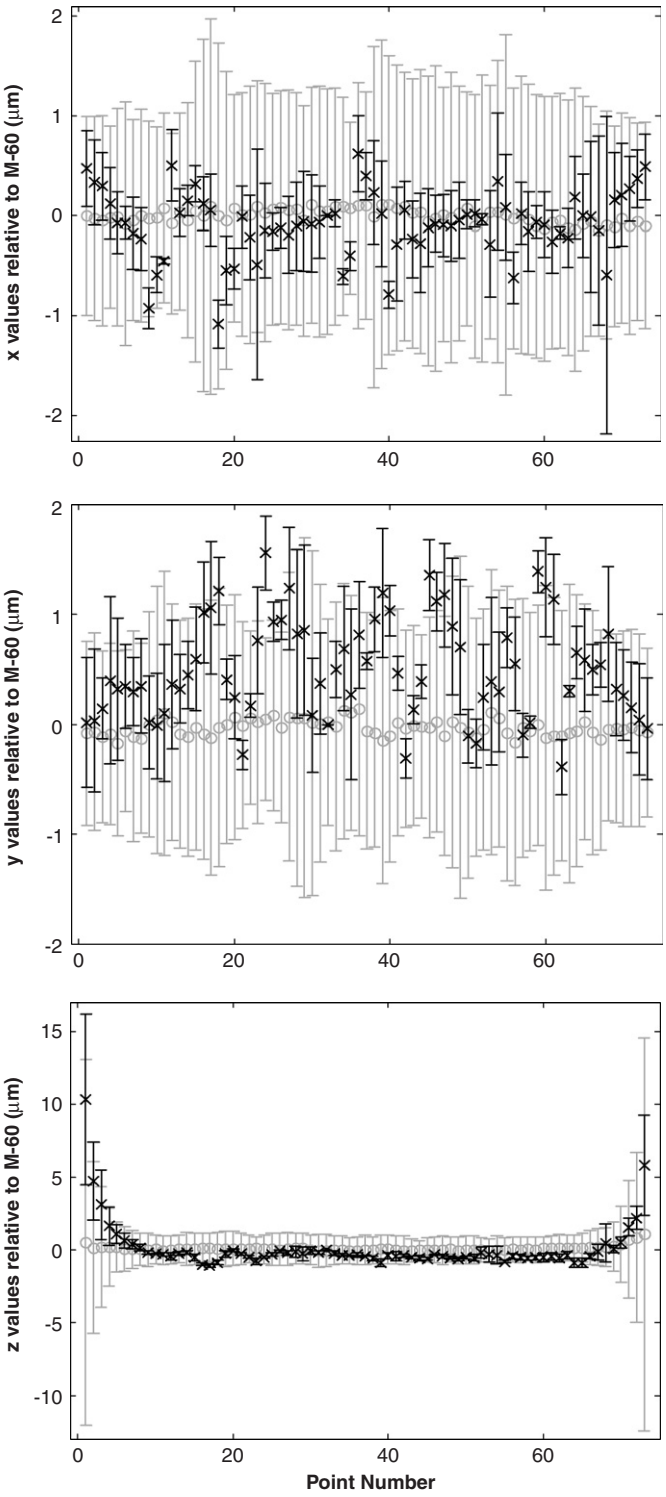

Fig. 7. LBB-CMM comparison, including simulation results and error bars.

6. Results and discussion

As noted, measurements were performed to compare spatial coordinates recorded by the LBB to those reported

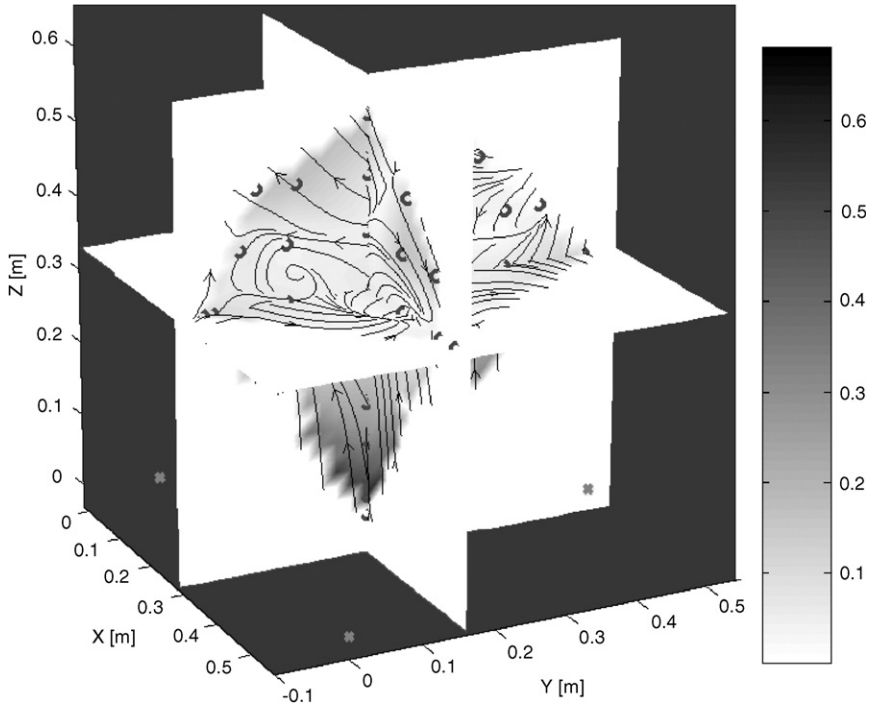

Fig. 8. Error magnitudes for simulated versus commanded positions within full work volume. The points from Fig. 6 and base socket locations are also identified.

by the Y-12 Moore M-60 CMM.[1] Both the CMM and LBB were housed in a temperature-controlled environment ($\pm 0.01\,^{\circ}C$) that was allowed to equilibrate prior to data collection (~ 1.5 h). In these tests, the three base socket distances were first measured, then the gantry-type Cartesian CMM was commanded to move to a set of 75 points within the LBB's work volume (defined by the base socket placements on the CMM worktable—an equilateral triangle arrangement was used with side lengths of 564 mm—and the tool socket location—mounted in place of the CMM probe) to record one of the base-to-tool socket lengths. This step was completed three times to obtain all three required base-to-tool socket lengths. The coordinates of each point were then computed by trilateration and the LBB and CMM results recorded. This sequence was completed three times. The 75 measurement points are identified in Fig. 6. The coordinates of the extreme points (in the LBB frame) are provided in Table 2.

Test results are shown in Fig. 7. This figure includes, for the x, y, and z directions (top to bottom), the difference between the LBB mean and CMM mean and the 2σ uncertainty bounds (the standard deviation of three trials for each measurement point multiplied by a coverage factor of 2) and Monte Carlo simulation mean difference and 2σ uncertainty. It is seen that the Monte Carlo analysis error bars encompass the CMM mean in all cases and overlap with the LBB error bars in all but three instances (96% agreement). This may be due to the limited number (3) of experimental data points. For the y and z experimental results, small biases are seen in the LBB mean values, e.g., the LBB y values generally lie above the mean simulation (and M-60) values. This can be explained by the fact that, in practice, the LBB uses the DMI value rather than the true length between sphere centers (calculated here using the HTM formulation) to compute the tool socket coordinates.

To further verify the simulation results, the LBB trilateration performance over the full work volume was predicted and analyzed. Fig. 8 gives the mean magnitude, defined by the vector difference between the mean simulated and commanded positions, and direction of the error throughout the measured work volume. Magnitude comparisons are shown using color variation and range from zero to 0.7 μm. The figure also demonstrates which coordinate direction dominates the errors in a region using an error flow field depicted by the streamlines with arrows. In those regions which exhibit the largest mean error, the model also predicts the largest standard deviation (i.e., the uncertainty is highest, 3.8 μm, at low z heights near the trilateration singularity location).

Finally, Fig. 9 compares the cumulative distributions of the error magnitudes from simulation and LBB measurements (provided in Fig. 7). The curves are normalized by dividing the bin amounts by the total sample set size. The agreement in these distributions suggests that the HTM

[1]The M-60 length standard measurement 2σ-uncertainty is $0.3\,\mu m + 0.4\,L$, where the length, L, is expressed in meters; probing errors are included. The x-axis positioning repeatability is 50 nm.

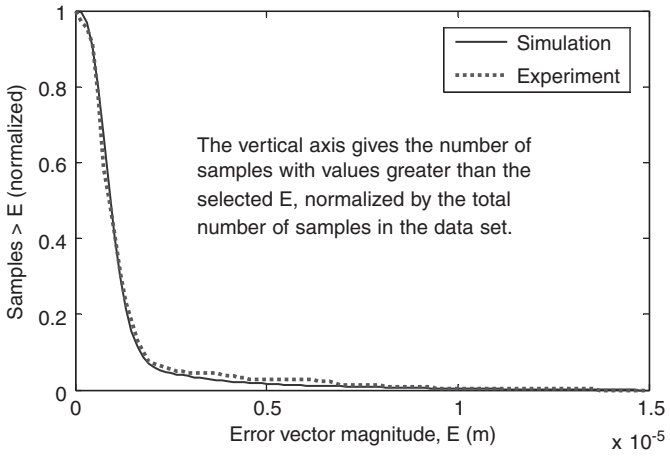

Fig. 9. Comparison of cumulative distributions for simulation and LBB measurements. The good agreement suggests a valid model.

model adequately describes the measurement and associated uncertainty.

7. Conclusions

An approach for developing uncertainty analyses for trilateration metrology was presented. Homogeneous transformation matrices were used to model the length uncertainty for the laser ball bar and Monte Carlo simulation was applied to determine the corresponding measurement uncertainty.

Acknowledgments

This work was supported in part by a grant from BWXT Y-12. The authors would also like to acknowledge helpful discussions with Dr. A. Davies, University of North Carolina at Charlotte, and Dr. R. Haftka, University of Florida.

References

[1] American National Standards Institute, (1997), ANSI/NCSL Z540-2-1997, US Guide to the Expression of Uncertainty in Measurement.
[2] S. Sandwith, R. Predmore, Real-time 5-micron uncertainty with laser tracking interferometer systems using weighted trilateration, in: Proceedings of the 2001 Boeing Large Scale Metrology Seminar, St. Louis, MO, 2001.
[3] W. Navidi, W.S. Murphy Jr., W. Hereman, Statistical methods in surveying by trilateration, Computational Statistics and Data Analysis 27 (1998) 209–227.
[4] M.C. Lee, P.M. Ferreira, Auto-triangulation and auto-trilateration. Part 2: three-dimensional experimental verification, Precision Engineering 26 (2002) 250–262.
[5] J.C. Ziegert, C.D. Mize, The laser ball bar: a new instrument for machine tool metrology, Precision Engineering 16 (4) (1994) 259–267.
[6] T.L. Schmitz, J.C. Ziegert, A new sensor for the micrometre-level measurement of three-dimensional dynamic contours, Measurement Science and Technology 10 (2) (1999) 51–62.
[7] A. Davies, T.L. Schmitz, defining the measurand in radius of curvature measurements, in: Proceedings of the 18th ASPE Annual Meeting, 26–31 October, Portland, OR, 2003 (on CD).
[8] N. Bobroff, Recent advances in displacement measuring interferometry, Measurement Science and Technology 4 (1993) 907–926.
[9] International Standards Organization (ISO), Guide to the Expression of Uncertainty in Measurement, 1993 (Corrected and Reprinted 1995).